

# Imaging-based Quantum Optomechanics

C. M. Pluchar,<sup>1</sup> W. He,<sup>1</sup> J. Manley,<sup>1</sup> N. Deshler,<sup>1</sup> S. Guha,<sup>1</sup> and D. J. Wilson<sup>1</sup>

<sup>1</sup>Wyant College of Optical Sciences, University of Arizona, Tucson, AZ 85721, USA

(Dated: July 10, 2024)

In active imaging protocols, information about a landscape is encoded into the spatial mode of a scattered photon. A common assumption is that the landscape is rigid; however, in principle it can be altered by radiation pressure, a concept that has found fruitful application in the field of quantum optomechanics. Here we explore active imaging of a mechanical resonator with an eye to generalizing the concept of radiation pressure backaction to spatially multimode light. As a thought experiment, we consider imaging the flexural modes of a membrane by sorting the spatial modes of a laser reflected from its surface. We show that backaction in this setting arises from spatial photon shot noise, an effect that cannot be observed in single-mode optomechanics. We also derive the imprecision-backaction product for coherent illumination in the limit of purely spatial backaction, revealing it to be equivalent to the standard quantum limit for purely dispersive, single-mode optomechanical coupling. Finally, we show that optomechanical correlations due to spatial backaction can give rise to two-mode entangled light. In conjunction with high- $Q$  nanomechanics, our findings point to new opportunities at the interface of quantum imaging and optomechanics, including sensors and networks enhanced by spatial mode entanglement.

Active imaging protocols are ubiquitous in science and technology, and play a key role in the development of quantum optics. A canonical example is the two-slit experiment, in which a simple landscape (a pair of slits) is encoded in the spatial distribution of photons on a screen [1]. Recent years have recast the two-slit experiment as one of a broader class of problems in quantum imaging [2, 3], which pursues techniques to enhance image resolution using nonclassical states of light [2, 4–7]. As a subclass of quantum metrology, quantum imaging has become an important testbed for quantum information theory [8]. It has also inspired diverse applications in fields from microscopy [9, 10] to astronomy [11].

In both classical and quantum imaging, a common assumption is that the landscape is rigid, in the sense that backaction due to radiation pressure can be ignored. This assumption is valid for most applications; however, it stands in basic contrast to treatments of interferometric displacement measurement in quantum optomechanics [12], for which backaction was early recognized as both a limitation [13] and a resource. Applied to mechanical resonators coupled to optical cavities, radiation pressure backaction has proven remarkably fruitful in the last two decades, leading to demonstrations of cooling of mechanical oscillators to the motional ground state [14], ponderomotive light squeezing [15], and displacement measurements at and below the standard quantum limit (SQL) [16]. In all of these demonstrations, the basic resource is radiation pressure shot noise in a single spatial mode of a laser field.

In this Letter, we explore active imaging of a mechanical resonator with a strong laser field, with an eye to extending the concept of radiation pressure backaction to spatially multi-mode light. A key motivation for our study is the emergence of ultra-high- $Q$  levitated and tethered nanomechanical resonators for which the use of scattering-based imaging is approaching the backaction regime [17–19]. Aside from alleviating practical constraints posed by optical cavities, the prospect of backaction-limited imaging offers intriguing opportunities at the interface of quantum imaging and quantum optomechanics, including the application and generation of spatially entangled light, using ponderomotive effects.

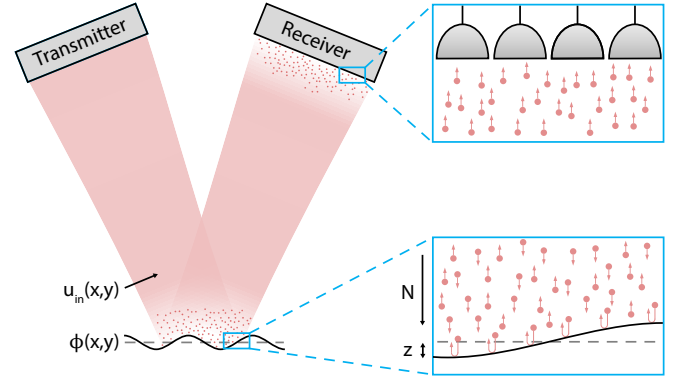


FIG. 1. Imprecision and backaction in active imaging of a vibrating membrane. Spatiotemporal fluctuations of the field at the detector (receiver) contribute imprecision noise. The same fluctuations produce radiation pressure backaction at the membrane surface.

The basic effect we wish to explore is radiation pressure backaction due to spatial photon shot noise. To illustrate this concept, we consider the thought experiment in Fig. 1, in which a vibrating membrane is illuminated by a laser beam (transmitter) and the reflected beam is imaged on a generic photoreceiver. Even if the intensity-averaged membrane displacement is zero, a spatially uncorrelated radiation pressure yields a nonzero generalized force spectral density [19–21]

$$S_F^{\text{BA}} = 8\hbar^2 k^2 \beta^2 N, \quad (1)$$

where  $N(k)$  is the laser photon flux (wavenumber) and

$$\beta^2 = \iint |u_{\text{in}}(x,y)|^2 \phi^2(x,y) dx dy, \quad (2)$$

is a unitless overlap factor between the normalized transverse modeshape of the laser  $u_{\text{in}}$  and the membrane  $\phi$ , respectively.

For a generic receiver, it can furthermore be shown that

$$S_z^{\text{imp}} S_F^{\text{BA}} \geq \hbar^2, \quad (3)$$

where  $S_z^{\text{imp}}$  is the apparent membrane displacement ( $z$ ) spectral density due to photon shot noise.

The imprecision-backaction product in Eq. 3 corresponds to the SQL for continuous readout of a harmonic oscillator [22], and can be derived from a heuristic semi-classical model that assumes the photon flux is random in both space and time (see Appendix [21]). Notably, it implies the existence of an optimal receiver [23] even if the average phase shift of the reflected field is zero, corresponding to zero optomechanical coupling in conventional single-mode cavity optomechanics [12]. A simple example is probing the angular displacement of the membrane near one of its vibrational nodes, for which the optimal receiver is one of a variety of beam displacement sensors (e.g., a lateral effect photodiode [24]). A non-trivial example is readout of a high order membrane vibration, which can be achieved using a spatial mode sorter [25] or structured homodyne receiver [26], as discussed below.

To formally derive Eqs. 1-3, we now develop a Hamiltonian description of our thought experiment. The essence of this approach, illustrated in Fig. 2, is to decompose the incident and reflected fields into orthogonal spatio-temporal modes, and to determine the energetic coupling between these modes, mediated by the membrane. Specializing to normal incidence, the spatial mode of the reflected field can be expressed as

$$u_{\text{in}} e^{2ikz\phi} \approx u_{\text{in}} + 2ikz\beta u_{\text{sc}} \quad (4a)$$

$$= u_{\text{in}} + 2ikz(\beta_{\parallel} u_{\text{in}} + \beta_{\perp} u_{\perp}) \quad (4b)$$

where  $u_{\text{sc}} = \beta^{-1} u_{\text{in}} \phi$  is the spatial mode of the scattered field and  $\{u_{\text{in}}, u_{\perp}\}$  form an orthonormal basis with inner product  $\langle u, v \rangle \equiv \iint u^* v dx dy$ . Assuming the incident and scattered fields are temporally orthogonal (confined to frequencies near the laser carrier  $\omega_0$  and motional sidebands  $\omega_0 \pm \omega_m$ , respectively), the interaction Hamiltonian can be expressed as

$$\hat{H}_{\text{int}} = 2\hbar k\beta(\hat{a}_{\text{in}}\hat{a}_{\text{sc}}^{\dagger} + \hat{a}_{\text{in}}^{\dagger}\hat{a}_{\text{sc}})\hat{z} \quad (5a)$$

$$= 2\hbar k[\beta_{\parallel}(\hat{a}_{\text{in}}\hat{a}_{\parallel}^{\dagger} + \hat{a}_{\text{in}}^{\dagger}\hat{a}_{\parallel}) \quad (5b)$$

$$+ \beta_{\perp}(\hat{a}_{\text{in}}\hat{a}_{\perp}^{\dagger} + \hat{a}_{\text{in}}^{\dagger}\hat{a}_{\perp})]\hat{z} \quad (5c)$$

where  $\hat{z}$  is the membrane displacement operator and  $\hat{a}$  is the annihilation operator for each optical mode, normalized so that  $\langle \hat{a}^{\dagger} \hat{a} \rangle$  is the photon flux (see Appendix [21]). For a laser in a strong coherent state,  $\hat{a}_{\text{in}} \rightarrow \sqrt{N} + \hat{a}_{\text{in}}$  [27], it follows that

$$\hat{H}_{\text{int}} \approx 2\hbar k\beta\sqrt{N}\hat{X}_{\text{sc}}\hat{z} \equiv \hat{F}_{\text{BA}}\hat{z}, \quad (6)$$

where  $\hat{X}_{\text{sc}} = \hat{a}_{\text{sc}} + \hat{a}_{\text{sc}}^{\dagger}$  and  $\hat{F}_{\text{BA}}$  are operators for the scattered field amplitude and radiation pressure force, respectively.

Equation 5 (and its linearized form, Eq. 6) is similar to the canonical optomechanical Hamiltonian [12], but is generalized to include the possibility of scattering into different spatial modes,  $\beta_{\perp} \neq 0$ . A key insight from Eq. 6 is that radiation pressure backaction occurs due to mixing of the coherent laser field with vacuum fluctuations of the orthogonal mode  $u_{\perp}$ . For single (spatial) mode optomechanical coupling  $\beta_{\perp} = 0$ , the scattered field is only temporally orthogonal, corresponding to a stochastic radiation pressure produced by random photon arrival times on the membrane surface. For purely spatial optomechanical coupling  $\beta_{\parallel} = 0$ , radiation pressure backaction can be interpreted as arising from random photon arrivals in

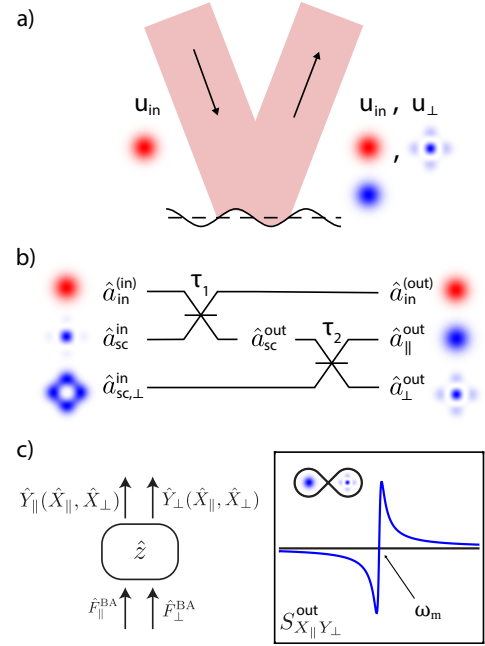


FIG. 2. Modal picture of spatio-temporal optomechanical coupling. (a) Reflection of a laser from a vibrating surface yields three spatio-temporally orthogonal modes (red and blue indicate frequency content near the laser carrier and motional sidebands frequencies, respectively). (b) Beamsplitter model for the interaction, with splitting ratios  $\tau_1(\omega) = 2k\beta_z(\omega)$  and  $\tau_2 = \beta_{\parallel}/\beta_{\perp}$ .  $\hat{a}_{\text{sc},\perp}$  represents sidebands in the orthogonal complement of  $u_{\text{sc}}$ . (c) Left: Schematic of optomechanical entanglement.  $\hat{F}_{\parallel(\perp)}^{\text{BA}} = 2\hbar k\beta_{\parallel(\perp)}\hat{X}_{\parallel(\perp)}^{\text{in}}$  is the temporal (spatial) component of the backaction force (Eq. 6). Right: Correlation spectrum between quadratures of the entangled modes (Eq. 11).

space. In general ( $\beta_{\perp} \neq 0$ ), it is attributable to a combination of spatial and temporal photon shot noise.

Equation 6 also gives insight into receiver architectures (Fig. 3). Specifically, for coherent illumination, displacement is encoded into the phase of the scattered field, as can be seen by computing the input-output relation (see Appendix [21])

$$\hat{a}_{\text{sc}}^{\text{out}}(t) = \hat{a}_{\text{sc}}^{\text{in}}(t) + 2i\hbar k\beta\sqrt{N}\hat{z}(t). \quad (7)$$

where  $\hat{a}_{\text{sc}}^{\text{out}}$  ( $\hat{a}_{\text{sc}}^{\text{in}}$ ) represent the field after (before) reflection. A known optimal receiver [23] in this context is a “structured” homodyne interferometer [18, 26] with a local oscillator mode  $u_{\text{LO}} = u_{\text{sc}}$ . An alternative is a spatial mode sorter configured to distill  $u_{\text{sc}}$  [25, 28, 29], following by direct detection.

Focusing on the structured homodyne receiver, which can access all quadratures of the scattered field, it is interesting to consider how imprecision, backaction, and their correlation—ponderomotive squeezing in single-mode optomechanics—manifest in the case of multimode optomechanical coupling  $u_{\text{in}} \neq u_{\text{sc}}$ . We thus consider the frequency-domain optomechanical equations of motion (see Appendix [21])

$$\hat{X}_{\text{sc}}^{\text{out}}(\omega) = \hat{X}_{\text{sc}}^{\text{in}}(\omega), \quad (8a)$$

$$\hat{Y}_{\text{sc}}^{\text{out}}(\omega) = \hat{Y}_{\text{sc}}^{\text{in}}(\omega) - 4k\beta\sqrt{N}\hat{z}(\omega), \quad \text{and} \quad (8b)$$

$$\hat{z}(\omega) = \chi(\omega)(F_{\text{th}}(\omega) + \hat{F}_{\text{BA}}(\omega)) \quad (8c)$$

$$= \chi(\omega)\left(F_{\text{th}}(\omega) - 4\hbar k\beta\sqrt{N}\hat{X}_{\text{sc}}^{\text{in}}(\omega)\right), \quad (8d)$$

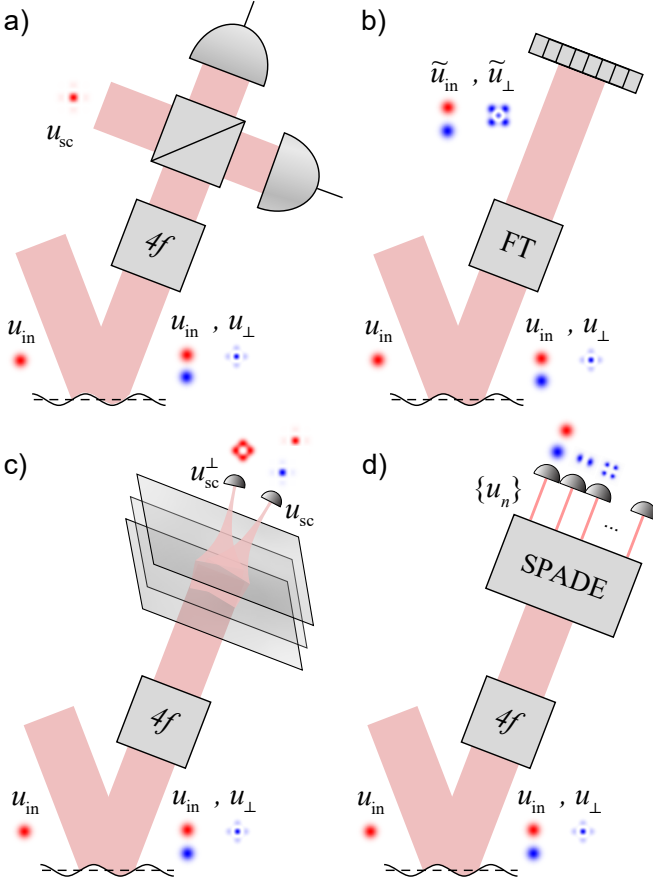


FIG. 3. Receivers for multimode optomechanical coupling. (a) A “structured” homodyne interferometer with its local oscillator in the scattered mode (a  $4f$  system compensates for diffraction.) (b) An appropriately weighted pixel array in the far field (equivalently, after taking the spatial Fourier Transform, FT) [21]. (c) A reconfigurable spatial mode sorter (SPADE) designed to distill the scattered mode. (d) A static SPADE sorting in an orthogonal (e.g., HG) basis.

where  $\hat{Y}_{sc} = i(\hat{a}_{sc}^\dagger - \hat{a}_{sc})$  is the phase quadrature of the scattered mode,  $\hat{X}_{sc}^{in}$  are  $\hat{Y}_{sc}^{in}$  are input vacuum noise,  $\chi$  is the mechanical susceptibility [21], and  $F_{th}$  is the thermal force.

For generic quadrature  $X_{sc}^\theta = X_{sc} \cos \theta + Y_{sc} \sin \theta$  with noise spectrum  $S_{X_{sc}^\theta} = \cos^2 \theta S_{X_{sc}} + \sin^2 \theta S_{Y_{sc}} + 2 \sin(2\theta) \text{Re}[S_{X_{sc}Y_{sc}}]$  the apparent displacement spectral density  $S_z^\theta$  is given by

$$S_z^\theta = \frac{S_{X_{sc}^\theta}^{\text{out}}}{16k^2\beta^2 N \sin^2 \theta} = S_z^{\text{imp}} + S_z^{\text{BA}} + S_z^{\text{imp,BA}} + S_z^{\text{th}} \quad (9)$$

where (noting  $S_{X_{sc}}^{\text{in}} = S_{Y_{sc}}^{\text{in}} = 2$ )  $S_z^{\text{imp}} = (8k^2\beta^2 N \sin^2 \theta)^{-1}$  is the measurement imprecision due to photon shot noise,  $S_z^{\text{BA(th)}} = |\chi|^2 S_F^{\text{BA(th)}}$  is the physical motion due to backaction (thermal) noise, and  $S_z^{\text{imp,BA}} = (4k^2\beta^2 N \tan \theta)^{-1} \text{Re}[S_{X_{sc}Y_{sc}}^{\text{out}}] = 4\hbar \cot \theta \text{Re}[\chi]$  is the imprecision-backaction cross-spectrum [21], corresponding to scattered mode quadrature correlations

$$S_{X_{sc}Y_{sc}}^{\text{out}} = -16\hbar k^2 \beta^2 N \chi. \quad (10)$$

Equation 9 is the general form for continuous linear displacement measurement of a mechanical oscillator [22], and

yields the SQL in the limit of no correlations  $S_z^{\text{imp,BA}} = 0$ , corresponding to phase quadrature readout ( $\theta = \pi/2$ ) and an imprecision-backaction saturating the lower bound of Eq. 3.

In the case that imprecision-backaction correlations do not vanish  $S_z^{\text{imp,BA}} \neq 0$ , the physical meaning of Eq. 9 depends on the form of optomechanical coupling. For purely dispersive coupling ( $\beta_\perp = 0$ ), it corresponds to quadrature squeezing of the illumination field due to the effective optomechanical Kerr nonlinearity (ponderomotive squeezing [12]). For purely spatial coupling ( $\beta_\parallel = 0$ ), the same interpretation holds, but the mode of the squeezed state is orthogonal to that of the input field. For a mixture of dispersive and spatial optomechanical coupling, the optomechanical interaction gives rise to a two-mode entangled state, manifesting as non-zero correlations between the quantum fluctuations of the two orthogonal spatial modes comprising the scattered field (a basic requirement for demonstrating inseparability between continuous-variable Gaussian states [30–32].) This can be seen by expressing Eq. 8 in terms of the  $\{\hat{a}_\parallel, \hat{a}_\perp\}$  mode quadratures,  $X_{sc}^\theta = \beta_\parallel X_\parallel^\theta + \beta_\perp X_\perp^\theta$ , yielding (see Appendix [21])

$$S_{X_\parallel Y_\perp}^{\text{out}} = -16\hbar k^2 \beta_\perp \beta_\parallel N \chi. \quad (11)$$

We now explore a concrete example illustrating the transition between dispersive and spatial optomechanical coupling. As shown in Fig. 4, we consider a square membrane vibrating in a symmetric mode  $\phi(x, y) = \cos(\pi x/\lambda_m) \cos(\pi y/\lambda_m)$  with nodal spacing  $\lambda_m$ . The laser beam is taken to be in the fundamental Hermite-Gauss (HG) mode  $u_{00}(x, y) = \sqrt{2/(\pi w_0^2)} e^{-((x-x_0)^2 + (y-y_0)^2)/w_0^2}$  with diameter  $2w_0 = 0.6\lambda_m$ . To visualize optomechanical coupling, we translate the beam position  $(x_0, y_0)$  while monitoring the scattered mode expansion in the co-translated HG basis

$$u_{sc} = \beta^{-1} \sum \langle u_{mn}, \phi u_{00} \rangle u_{mn} \equiv \beta^{-1} \sum \beta_{mn}(x_0, y_0) u_{mn} \quad (12)$$

noting that expansion coefficients  $\beta_{mn}$  satisfy  $\beta_\parallel = \beta_{00}$  and

$$\beta^2 = \sum |\beta_{mn}|^2. \quad (13)$$

As shown in Fig. 4(e), translating the laser beam between an antinode and a node of the membrane mode gives access to different scattered modes and optomechanical couplings. The case where the beam is centered on an antinode has been widely studied in the field of optomechanics and corresponds to mainly dispersive optomechanical coupling,  $\beta_\perp \ll \beta_\parallel$ . The case where the beam is centered on a node has been little explored, and corresponds to purely spatial optomechanical coupling  $\beta_\parallel = 0$ . In both cases, the magnitude of the overall coupling factor  $\beta$  depends on the beam diameter.

We first emphasize the case where the laser beam is positioned halfway between antinodes ( $x = \lambda_m/2$ ), so that the scattered mode is approximately  $\text{HG}_{10}$  ( $\beta_{10}^2 \approx 1$ ). In this case, when  $w_0 \ll \lambda_m$  ( $\beta_{10} \rightarrow 1$ ), the membrane’s motion can be modeled as an angular displacement  $\varphi = 2\pi z/\lambda_m$  and backaction can be treated as a torque  $\tau_{\text{BA}} = F_{\text{BA}} \lambda_m/2$ , satisfying

$$S_\varphi S_\tau \geq \hbar^2, \quad (14)$$

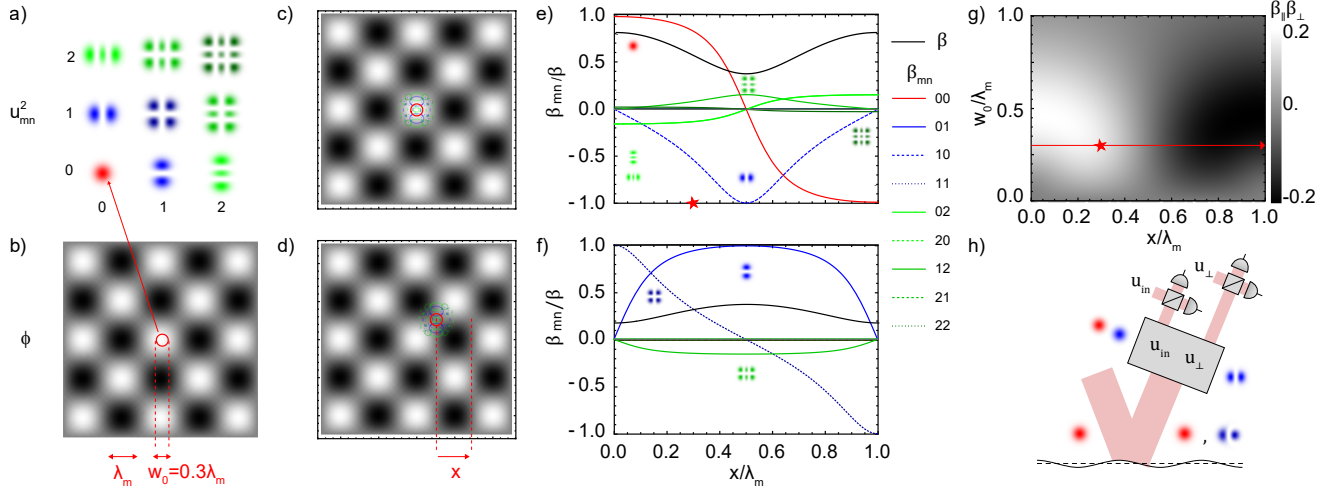


FIG. 4. Multimode optomechanical coupling to a membrane. (a) Hermite-Gauss (HG) mode intensity distributions  $u_{mn}^2(x,y)$ . (b) Mechanical mode shape  $\phi(x,y)$  with nodal spacing  $\lambda_m$ . The red circle represents the HG mode diameter  $2w_0$ . (c,d) Visualization of the overlap between  $u_{mn}$  and  $\phi$  when the beam is centered at an antinode (c) and node (d) of  $\phi$ . (e,f) Plots of the modal overlap factors  $\beta_{mn}$  for  $w_0 = 0.3\lambda_m$ , versus lateral offset  $x$  from the initial position in (c,d), respectively. (g) Density plot of  $\beta_{\perp}\beta_{\parallel}$  versus mode waist  $w_0$  and location  $x$  as in (c,e), encoding the magnitude of the correlations between  $Y_{\perp}^{\text{out}}$  and  $X_{\parallel}^{\text{out}}$  as described in Eq. 11. (h) Dual-homodyne receiver for characterizing correlations between parallel  $u_{\text{in}}$  and perpendicular  $u_{\perp}$  scattered mode quadratures, e.g.  $u_{\text{in}} = u_{00}$  and  $u_{\perp} \approx u_{01}$  for the starred position in (e) and (g).

as has been recently studied in the context of optical lever measurements on high- $Q$  nanomechanical resonators [19, 33].

As shown in Fig. 4e, translating the beam away from a node gives access to the more general case  $\beta_{\perp}\beta_{\parallel} \neq 0$ , corresponding to two-mode entanglement according to Eq. 11. For the highlighted (starred) position, if  $w_0 \ll \lambda_m$ , entanglement is distributed between  $u_{\text{in}} = u_{00}$  and  $u_{\perp} \approx u_{01}$ . This can be witnessed by performing a variational measurement [34] in which the  $u_{\text{in}}$  and  $u_{\perp}$  ports of a reconfigurable mode sorter are analyzed using independent homodyne interferometers, yielding measurements of  $X_{\perp}^{\theta, \text{out}}$  and  $X_{\parallel}^{\theta, \text{out}}$ , respectively. In Fig. 4g we plot  $\beta_{\perp}\beta_{\parallel}$  versus  $x$  and  $w_0$ , illustrating that correlations are maximized at positions between a node and antinode.

In summary, we have explored radiation pressure backaction in the context of active imaging of a mechanical resonator, presenting a Hamiltonian description that includes two forms of optomechanical coupling. In the first form, the incident and scattered field are in the same spatial mode ( $\beta_{\perp} = 0$ ), corresponding to traditional dispersive optomechanical coupling. In the second form, the incident and scattered modes are orthogonal ( $\beta_{\parallel} = 0$ ), corresponding to purely spatial optomechanical coupling. Backaction in both cases originates from mixing of the incident field with vacuum fluctuations of the scattered mode, giving rise to a radiation pressure force which is random in time (for dispersive coupling) and space (for spatial coupling). Recoil of the landscape gives rise to amplitude-phase correlations. For purely dispersive or spatial coupling, these correlations correspond to single-mode ponderomotive squeezing. In the intermediate case  $\beta_{\parallel}\beta_{\perp} \neq 0$ ,

they correspond to generation of two-mode entanglement.

Looking forward, advances in free-space optomechanics auger well for the study of spatial backaction, including recent demonstrations of ponderomotive squeezing with levitated nanospheres [35, 36] and high cooperativity deflectometry of nanobeams [19, 33]. To extend these experiments, insights might be drawn from a growing portfolio of “quantum-inspired” imaging protocols, such as super-resolution imaging [9, 10] with low-loss SPADE technology [25]. Entanglement-enhanced imaging is also naturally applicable to mechanical resonators, and provides a complementary approach to entanglement-enhanced distributed force sensing [37]. Finally, it is interesting to consider nanomechanical resonators as quantum imaging testbeds, since they provide a diversity of multi-parameter estimation problems, and a rubric for transceiver design, through the backaction-imprecision product (Eq. 3) [38]. Combining these considerations may usher in a new era of imaging-based quantum optomechanics.

## ACKNOWLEDGMENTS

The authors thank Allison Rubenok, Morgan Choi, and Ewan Wright for helpful discussions. This work was supported by the National Science Foundation (NSF) through award No. 2239735. CMP acknowledges support from the ARCS Foundation. WH and SG acknowledge support from Air Force Office of Scientific Research contract No. FA9550-22-1-0180. ND acknowledges support from the NSF Graduate Research Fellowship under Grant No. DGE-2137419.

[1] W. K. Wootters and W. H. Zurek, “Complementarity in the double-slit experiment: Quantum nonseparability and a quan-

titative statement of bohr’s principle,” *Phys. Rev. D* **19**, 473 (1979).

- [2] P.-A. Moreau, E. Toninelli, T. Gregory, and M. J. Padgett, “Imaging with quantum states of light,” *Nat. Rev. Phys.* **1**, 367–380 (2019).
- [3] L. A. Lugiato, A. Gatti, and E. Brambilla, “Quantum imaging,” *J. Opt. B: Quantum Semiclass. Opt.* **4**, S176 (2002).
- [4] N. Treps, U. Andersen, B. Buchler, P. K. Lam, A. Maitre, H.-A. Bachor, and C. Fabre, “Surpassing the standard quantum limit for optical imaging using nonclassical multimode light,” *Phys. Rev. Lett* **88**, 203601 (2002).
- [5] N. Treps, N. Grosse, W. P. Bowen, C. Fabre, H.-A. Bachor, and P. K. Lam, “A quantum laser pointer,” *Science* **301**, 940–943 (2003).
- [6] G. Brida, M. Genovese, and I. Ruo Berchera, “Experimental realization of sub-shot-noise quantum imaging,” *Nature Photonics* **4**, 227–230 (2010).
- [7] R. C. Pooser and B. Lawrie, “Ultrasensitive measurement of microcantilever displacement below the shot-noise limit,” *Optica* **2**, 393–399 (2015).
- [8] O. S. Magaña-Loaiza and R. W. Boyd, “Quantum imaging and information,” *Rep. Prog. Phys.* **82**, 124401 (2019).
- [9] M. Tsang, R. Nair, and X.-M. Lu, “Quantum theory of super-resolution for two incoherent optical point sources,” *Phys. Rev. X* **6**, 031033 (2016).
- [10] M. R. Grace and S. Guha, “Identifying objects at the quantum limit for superresolution imaging,” *Phys. Rev. Lett* **129**, 180502 (2022).
- [11] R. M. Lau, A. Ashok, J. Emms, D. R. Gies, S. Guha, Z. Hartman, B. McClinton, J. Monnier, J. K. Rajagopal, J. G. Richardson, et al., “Charting quantum horizons to establish a roadmap for microsecond astronomy,” *Nat. Astron.* **1–2** (2024).
- [12] M. Aspelmeyer, T. J. Kippenberg, and F. Marquardt, “Cavity optomechanics,” *Rev. Mod. Phys.* **86**, 1391 (2014).
- [13] C. M. Caves, “Quantum-mechanical noise in an interferometer,” *Phys. Rev. D* **23**, 1693 (1981).
- [14] M. Rossi, D. Mason, J. Chen, Y. Tsaturyan, and A. Schliesser, “Measurement-based quantum control of mechanical motion,” *Nature* **563**, 53–58 (2018).
- [15] T. P. Purdy, P.-L. Yu, R. W. Peterson, N. S. Kampel, and C. A. Regal, “Strong optomechanical squeezing of light,” *Phys. Rev. X* **3**, 031012 (2013).
- [16] D. Mason, J. Chen, M. Rossi, Y. Tsaturyan, and A. Schliesser, “Continuous force and displacement measurement below the standard quantum limit,” *Nat. Phys.* **15**, 745–749 (2019).
- [17] F. Tebbenjohanns, M. Frimmer, and L. Novotny, “Optimal position detection of a dipolar scatterer in a focused field,” *Phys. Rev. A* **100**, 043821 (2019).
- [18] F. Tebbenjohanns, A. Militaru, A. Norrman, F. van der Laan, L. Novotny, and M. Frimmer, “Optimal orientation detection of an anisotropic dipolar scatterer,” *Phys. Rev. A* **105**, 053504 (2022).
- [19] S. Hao and T. P. Purdy, “Back action evasion in optical lever detection,” *Optica* **11**, 10–17 (2024).
- [20] M. Pinard, Y. Hadjar, and A. Heidmann, “Effective mass in quantum effects of radiation pressure,” *Eur. Phys. J. D* **7**, 107–116 (1999).
- [21] See Supplemental Material.
- [22] A. A. Clerk, M. H. Devoret, S. M. Girvin, F. Marquardt, and R. J. Schoelkopf, “Introduction to quantum noise, measurement, and amplification,” *Rev. Mod. Phys.* **82**, 1155 (2010).
- [23] We define an optimal receiver as for which the imprecision-backaction product given by Equation 1 is minimized.
- [24] E. Fradgley, C. French, L. Rushton, Y. Dieudonné, L. Harrison, J. L. Beckey, H. Miao, C. Gill, P. Petrov, and V. Boyer, “Quantum limits of position-sensitive photodiodes,” *Opt. Express* **30**, 39374–39381 (2022).
- [25] P. Boucher, C. Fabre, G. Labroille, and N. Treps, “Spatial optical mode demultiplexing as a practical tool for optimal transverse distance estimation,” *Optica* **7**, 1621–1626 (2020).
- [26] H. Sun, K. Liu, Z. Liu, P. Guo, J. Zhang, and J. Gao, “Small-displacement measurements using high-order hermite-gauss modes,” *Appl. Phys. Lett.* **104** (2014).
- [27] Here and below, we define operators in a frame rotating at the laser carrier frequency,  $\omega_0$ .
- [28] N. K. Fontaine, R. Ryf, H. Chen, D. T. Neilson, K. Kim, and J. Carpenter, “Laguerre-gaussian mode sorter,” *Nat. Commun* **10**, 1865 (2019).
- [29] I. Ozer, M. R. Grace, and S. Guha, “Reconfigurable spatial-mode sorter for super-resolution imaging,” in *2022 CLEO Conference* (IEEE, 2022) pp. 1–2.
- [30] L.-M. Duan, G. Giedke, J. I. Cirac, and P. Zoller, “Inseparability criterion for continuous variable systems,” *Phys. Rev. Lett.* **84**, 2722 (2000).
- [31] J. Chen, M. Rossi, D. Mason, and A. Schliesser, “Entanglement of propagating optical modes via a mechanical interface,” *Nat. Commun* **11**, 943 (2020).
- [32] C. Fabre and N. Treps, “Modes and states in quantum optics,” *Rev. Mod. Phys.* **92**, 035005 (2020).
- [33] J. R. Pratt, A. R. Agrawal, C. A. Condos, C. M. Pluchar, S. Schlamminger, and D. J. Wilson, “Nanoscale torsional dissipation dilution for quantum experiments and precision measurement,” *Phys. Rev. X* **13**, 011018 (2023).
- [34] H. J. Kimble, Y. Levin, A. B. Matsko, K. S. Thorne, and S. P. Vyatchanin, “Conversion of conventional gravitational-wave interferometers into quantum nondemolition interferometers by modifying their input and/or output optics,” *Phys. Rev. D* **65**, 022002 (2001).
- [35] A. Militaru, M. Rossi, F. Tebbenjohanns, O. Romero-Isart, M. Frimmer, and L. Novotny, “Ponderomotive squeezing of light by a levitated nanoparticle in free space,” *Phys. Rev. Lett* **129**, 053602 (2022).
- [36] L. Magrini, V. A. Camarena-Chávez, C. Bach, A. Johnson, and M. Aspelmeyer, “Squeezed light from a levitated nanoparticle at room temperature,” *Phys. Rev. Lett* **129**, 053601 (2022).
- [37] Y. Xia, A. R. Agrawal, C. M. Pluchar, A. J. Brady, Z. Liu, Q. Zhuang, D. J. Wilson, and Z. Zhang, “Entanglement-enhanced optomechanical sensing,” *Nat. Photonics* **17**, 470–477 (2023).
- [38] M. Tsang, H. M. Wiseman, and C. M. Caves, “Fundamental quantum limit to waveform estimation,” *Phys. Rev. Lett* **106**, 090401 (2011).
- [39] M. Kim, L. Allen, and R. Loudon, “Quantum theory of radiation pressure on a dielectric slab,” *Phys. Rev. A* **50**, 3614 (1994).
- [40] R. Loudon, “Theory of the forces exerted by laguerre-gaussian light beams on dielectrics,” *Phys. Rev. A* **68**, 013806 (2003).
- [41] P. Samphire, R. Loudon, and M. Babiker, “Quantum theory of radiation-pressure fluctuations on a mirror,” *Phys. Rev. A* **51**, 2726 (1995).
- [42] A. Wünsche, “Quantization of gauss-hermite and gauss-laguerre beams in free space,” *J. Opt. B: Quantum Semiclass. Opt.* **6**, S47 (2004).
- [43] K. Blow, R. Loudon, S. J. Phoenix, and T. Shepherd, “Continuum fields in quantum optics,” *Phys. Rev. A* **42**, 4102 (1990).
- [44] C. W. Gardiner and M. J. Collett, “Input and output in damped quantum systems: Quantum stochastic differential equations and the master equation,” *Phys. Rev. A* **31**, 3761 (1985).
- [45] P. R. Saulson, “Thermal noise in mechanical experiments,” *Phys. Rev. D* **42**, 2437 (1990).

## APPENDIX

This appendix provides extended derivations of Eqs. 1 - 11.

### I. SPATIOTEMPORAL SHOT NOISE: SEMICLASSICAL MODEL

Consider a laser beam with mean photon flux  $N$  (units  $s^{-1}$ ) focused onto a surface in the  $x-y$  plane. The photon intensity on the surface (units  $s^{-1}m^{-2}$ ) can be expressed as

$$I_{\text{in}}(x, y) = N |u_{\text{in}}(x, y)|^2 \quad (15)$$

where  $u_{\text{in}}(x, y)$  is the transverse beam modeshape with normalization  $\iint dxdy |u_{\text{in}}(x, y)|^2 = 1$ .

Semiclassically, photon shot noise can be modeled as a spatiotemporally random intensity fluctuation  $\delta I_{\text{in}}^{\text{shot}}(t, x, y)$  with single-sided cross spectral density (PSD)

$$S_{I, I'}^{\text{in, shot}} = 2I_{\text{in}}(x, y) \delta(x-x') \delta(y-y') \quad (16)$$

As a consistency check, note that the mean photon flux through a subsurface  $A$  is  $N_A = \iint_A dxdy I_{\text{in}}(x, y)$  and that shot noise contributes temporal fluctuations  $\delta N_A^{\text{shot}}(t) = \iint_A dxdy \delta I_{\text{in}}^{\text{shot}}(t, x, y)$  through this subsurface with PSD

$$S_{N_A}^{\text{shot}} = \iint_A dxdy \iint_A dx'dy' S_{I, I'}^{\text{in, shot}} = 2N_A, \quad (17)$$

which is the standard result for temporal shot noise [22].

#### A. Generalized Radiation Pressure Backaction

We now consider the influence of shot noise on active imaging of a compliant landscape, starting with measurement backaction. Towards this end, following Fig. 1, suppose the laser is focused onto a perfectly reflective membrane vibrating in a transverse mode with amplitude  $z_{\text{m}}(x, y, t) = z_0(t)\phi(x, y)$ . Photon shot noise imparts a spatiotemporally random radiation pressure  $\delta P_{\text{rad}}^{\text{shot}}(t, x, y) = 2\hbar k \delta I_{\text{in}}(t, x, y)$  on the membrane with cross spectral density  $S_{P, P'}^{\text{rad, shot}} = 4\hbar^2 k^2 S_{I, I'}^{\text{in, shot}}$ , where  $k$  is the laser wavenumber. The resulting generalized backaction force on the membrane mode is given by

$$F_{\text{BA}}(t) = \iint dxdy \phi(x, y) \delta P_{\text{rad}}^{\text{shot}}(t, x, y). \quad (18)$$

The associated force PSD is given by

$$S_F^{\text{BA}} = \iiint dxdy dx' dy' \phi(x, y) \phi(x', y') S_{P, P'}^{\text{rad, shot}} \quad (19a)$$

$$= 8\hbar^2 k^2 \beta^2 N \quad (19b)$$

with

$$\beta^2 \equiv \iint dxdy \phi^2(x, y) |u_{\text{in}}(x, y)|^2. \quad (20)$$

### B. Imprecision Noise and Receiver Ideality

Shot noise also gives rise to imprecision in an imaging-based estimate of the membrane displacement  $z_0$ , with a magnitude that depends on the receiver architecture. The receivers in Fig. 3 all infer  $z_0$  from the complex amplitude of the reflected field, given for small displacement ( $kz_0 \ll 1$ ) as

$$E_{\text{ref}}(x, y) = E_{\text{in}}(x, y) e^{i2kz_0 \phi(x, y)} \quad (21a)$$

$$\approx A_{\text{in}} (u_{\text{in}}(x, y) + i2\beta k z_0 u_{\text{sc}}(x, y)) \quad (21b)$$

where  $A_{\text{in}} = \sqrt{2\eta \hbar k c N} e^{i\theta_{\text{in}}}$  is the incident field amplitude,  $\eta$  is the electromagnetic impedance, and  $u_{\text{sc}}(x, y) \equiv u_{\text{in}}(x, y)\phi(x, y)/\beta$  is the modeshape of the scattered field. Below we explore two examples: a structured homodyne interferometer (Fig. 3a) and a pixelated camera in the far field (Fig. 3b). We show that both receivers are ideal in the sense that their displacement imprecision  $z_{\text{imp}}$  due to shot noise saturates the Standard Quantum Limit (SQL):  $S_z^{\text{imp}} S_F^{\text{BA}} = \hbar^2$ .

#### 1. Structured Homodyne Interferometer

In a structured homodyne interferometer, the reflected field is combined on a 50:50 beamsplitter with a local oscillator field  $E_{\text{LO}}(x, y) = A_{\text{LO}} u_{\text{LO}}(x, y)$  with amplitude  $A_{\text{LO}} = e^{i\theta_{\text{LO}}} \sqrt{2\eta \hbar k c N_{\text{LO}}}$  and modeshape  $u_{\text{LO}}$ . Balanced detection of the beamsplitter outputs yields a photocurrent

$$i_{\text{hom}} = 4kz_0 \beta \xi \sqrt{N_{\text{LO}} N} \langle u_{\text{LO}}, u_{\text{sc}} \rangle \sin(\theta_{\text{LO}} - \theta_{\text{in}}) \quad (22a)$$

$$\leq 4kz_0 \beta \sqrt{N_{\text{LO}} N} \quad (22b)$$

where  $\xi$  is the photodetection efficiency. The upper bound is achieved when  $\xi = 1$ ,  $u_{\text{LO}} = u_{\text{sc}}$  and  $\theta_{\text{LO}} - \theta_{\text{in}} = \pi/2$ .

To determine  $S_z^{\text{imp}}$ , we refer the photocurrent shot noise  $S_i^{\text{hom, shot}} = 2\xi(N_{\text{LO}} + N)$  to an apparent displacement

$$S_z^{\text{imp}} \equiv \left( \frac{di_{\text{hom}}}{dz_0} \right)^{-2} S_i^{\text{hom, shot}} \geq \frac{1}{8k^2 \beta^2 N} \quad (23)$$

with the lower bound achieved with the above parameters and a strong local oscillator,  $N_{\text{LO}} \gg N$ . Comparison with Eq. 19 reveals this bound to saturate the SQL:  $S_z^{\text{imp}} = \hbar^2 / S_F^{\text{BA}}$ .

#### 2. Pixelated camera in the far field

Consider a pixelated camera imaging the reflected field in the far field as shown in Fig. 3b—i.e., at a distance  $d \gg kw_0^2$  from the membrane, where  $w_0$  is the laser spot size. Using Fraunhofer's diffraction formula

$$I(x, y) \approx \frac{N}{\lambda^2 d^2} \left( |\tilde{u}_{\text{in}}|^2 - 4\beta k z_0 \text{Im} \{ \tilde{u}_{\text{sc}} \tilde{u}_{\text{in}}^* \} \right) \quad (24)$$

where  $\tilde{u}(x, y) = \iint dx' dy' e^{-ik(xx'+yy')/d} u(x', y')$ .

Information about  $z_0$  is encoded in the photocurrent produced by each pixel,  $i_{mn}$ . Assuming small, square pixels with

side length  $l$  and coordinates  $(x_m, y_n)$  in the detector plane, the photocurrent mean and fluctuations can be approximated as

$$\bar{i}_{mn} = \frac{N\xi}{\lambda^2 d^2} |\tilde{u}_{in,mn}|^2 l^2 \quad \text{and} \quad (25a)$$

$$\delta i_{mn}(t) = -4\beta k z_0(t) \frac{N\xi}{\lambda^2 d^2} B_{mn} l^2 + \delta i_{mn}^{\text{shot}}(t) \quad (25b)$$

respectively, where subscript  $mn$  denotes evaluation at position  $(x_m, y_n)$ ,  $B_{mn} \equiv \text{Im} \left\{ \tilde{u}_{sc,mn} \tilde{u}_{in,mn}^* \right\}$ , and  $\delta i_{mn}^{\text{shot}}$  is the photocurrent shot noise with PSD  $S_{\delta i_{mn}^{\text{shot}}} = 2\bar{i}_{mn}$ .

To make an estimate  $z_0^{\text{est}}$  of  $z_0$ , the sum of squared residual photocurrents can be minimized, weighted by the shot noise inverse variance, viz.

$$\text{Min} \sum_{mn} \sigma_{i_{mn}, \text{shot}}^{-2} \left( \frac{\partial i_{mn}}{\partial z_0} z_0^{\text{est}} - \delta i_{mn} \right)^2 \quad (26)$$

where

$$\sigma_{i_{mn}, \text{shot}}^2 = S_{\delta i_{mn}^{\text{shot}}} \Delta f = 2\bar{i}_{mn} \Delta f \quad (27)$$

is the variance of the pixel shot noise in bandwidth  $\Delta f$ .

The solution to Eq. 26,  $z_0^{\text{est}} = z_0 + z_{\text{imp}}$ , has an imprecision

$$z_{\text{imp}} = \left( \sum_{mn} \sigma_{i_{mn}, \text{shot}}^{-2} \left( \frac{\partial i_{mn}}{\partial z_0} \right)^2 \right)^{-1} \sum_{mn} \sigma_{i_{mn}, \text{shot}}^{-2} \frac{\partial i_{mn}}{\partial z_0} \delta i_{mn}^{\text{shot}} \quad (28)$$

To compute  $S_z^{\text{imp}}$ , we note that shot noise is uncorrelated between pixels and take the continuum limit  $l \rightarrow 0$ . A straightforward calculation reveals  $S_z^{\text{imp}} = \kappa \hbar^2 / S_F^{\text{BA}}$ , where

$$\begin{aligned} \kappa &\equiv \lambda^2 d^2 \left( \iint dxdy \frac{(\text{Im} [\tilde{u}_{sc}(x,y) \tilde{u}_{in}^*(x,y)])^2}{|\tilde{u}_{in}(x,y)|^2} \right)^{-1} \\ &= \lambda^2 d^2 \left( \frac{\beta_{\perp}}{\beta} \right)^2 \left( \iint dxdy \frac{(\text{Im} [\tilde{u}_{\perp}(x,y) \tilde{u}_{in}^*(x,y)])^2}{|\tilde{u}_{in}(x,y)|^2} \right)^{-1} \end{aligned} \quad (29)$$

is a unitless ideality factor and  $u_{\perp}$  is the orthogonal component of  $u_{sc}$  ( $\beta u_{sc} = \beta_{\perp} u_{\perp} + \beta_{\parallel} u_{in}$ ) as defined in the main text.

Equation 29 implies that the ideality of the far-field camera receiver depends on the relationship between the input  $u_{in}$  and scattered  $u_{sc}$  modeshapes—i.e., the nature of the optomechanical coupling. For example, the camera provides no displacement information ( $\kappa = \infty$ ) in the case of purely dispersive coupling,  $u_{sc} = u_{in}$ . It can however perform an ideal measurement ( $\kappa = 1$ ) on a rotating surface ( $\phi \propto x$ ) when the input field is a fundamental Gaussian beam. This can be seen by noting that  $\tilde{u}_{in}$  is real-valued (because it is an even function of  $x$  and  $y$ ) while  $\tilde{u}_{sc}$  is purely imaginary (because  $u_{sc} \propto x u_{in}$  is an odd function in  $x$  and an even function in  $y$ ). Therefore,  $\kappa$  simplifies to  $\lambda^{-2} d^{-2} \iint dxdy |\tilde{u}_{sc}(x,y)|^2$ , which by Plancherel's theorem is simply  $\kappa = \iint dxdy |u_{sc}(x,y)|^2 = 1$ .

## II. HAMILTONIAN TREATMENT

We now derive the effective Hamiltonian for the optomechanical interaction discussed in the main text (Eqs. 5-6).

Following the above treatment, we consider a perfectly reflective membrane located at  $z = 0$ , vibrating in a transverse mode with amplitude  $z_m(x,y,t) = z_0(t)\phi(x,y)$ . We assume a monochromatic laser beam is incident on the membrane from the left ( $z < 0$ ). The electromagnetic field  $\{\mathbf{E}, \mathbf{B}\}$  in this domain is a closed system with classical Hamiltonian,

$$H_{\text{EM}} = \int_{-\infty}^{\infty} \int_{-\infty}^{\infty} dxdy \int_{-\infty}^{z_m} \left( \frac{\epsilon_0 \mathbf{E}(\mathbf{r})^2}{2} + \frac{\mathbf{B}(\mathbf{r})^2}{2\mu_0} \right) dz, \quad (30)$$

where  $\epsilon_0$  ( $\mu_0$ ) is the permittivity (permeability) of free space. For sufficiently small  $z_m$ , we can approximate

$$H_{\text{EM}} \approx \iint dxdy \int_{-\infty}^0 \left( \frac{\epsilon_0 \mathbf{E}(\mathbf{r})^2}{2} + \frac{\mathbf{B}(\mathbf{r})^2}{2\mu_0} \right) dz \quad (31a)$$

$$+ z_0 \iint dxdy \left( \frac{\epsilon_0 \mathbf{E}(x,y,0)^2}{2} + \frac{\mathbf{B}(x,y,0)^2}{2\mu_0} \right) \phi(x,y) \quad (31b)$$

$$\equiv H_{\text{EM}}^{\text{free}} + H_{\text{int}}, \quad (31c)$$

where  $H_{\text{EM}}^{\text{free}}$  (Eq. 31a) describes the free field evolution and  $H_{\text{int}}$  (Eq. 31b) describes the optomechanical interaction.

We now wish to quantize  $H_{\text{EM}}$ . To this end, following a standard approach [39–41], we quantize the paraxial fields in the half-space  $z < 0$  [40], assuming normal incidence and the boundary condition  $E(x,y,0) = 0$  for a perfect reflector:

$$\hat{\mathbf{E}}(\mathbf{r}, t) = -\mathbf{e} \sum_n \int_0^{\infty} d\omega \sqrt{\frac{\hbar\omega}{\pi\epsilon_0 c}} (\hat{a}_n(\omega) U_{kn}(\mathbf{r}) e^{-i\omega t} + \text{h.c.}) \sin(kz) \quad (32a)$$

$$\hat{\mathbf{B}}(\mathbf{r}, t) = \frac{i}{c} \mathbf{b} \sum_n \int_0^{\infty} d\omega \sqrt{\frac{\hbar\omega}{\pi\epsilon_0 c}} (\hat{a}_n(\omega) U_{kn}(\mathbf{r}) e^{-i\omega t} - \text{h.c.}) \cos(kz). \quad (32b)$$

Here  $\mathbf{b} = \mathbf{e} \times \mathbf{k}/k$  is the magnetic field polarization,  $\omega = kc$  is the optical frequency,  $U_{kn}(\mathbf{r}) = e^{iz\sqrt{1/k}} u_n(x,y)$  [42] is a transverse-orthonormal basis for Gaussian beams satisfying

$$\iint U_{kn} U_{k'n'}^* dxdy = \iint u_n u_{n'}^* dxdy = \delta_{nn'}, \quad (33)$$

and  $\hat{a}_n[\omega]$  is a bosonic operator with commutation relation  $[\hat{a}_n[\omega], \hat{a}_{n'}^{\dagger}[\omega']] = \delta_{n,n'} \delta[\omega - \omega']$  normalized so that  $\sum_n \int \hat{a}_n^{\dagger}[\omega] \hat{a}_n[\omega] d\omega$  and  $\frac{1}{2\pi} \sum_n \iint \hat{a}_n^{\dagger}[\omega] \hat{a}_n[\omega'] e^{-i(\omega - \omega')t} d\omega d\omega'$  are the total photon number and flux, respectively [43].

A straightforward calculation using Eqs. 32-33 and the rotating wave approximation (RWA) then yields

$$\hat{H}_{\text{EM}}^{\text{free}} = \sum_n \hbar \int_0^{\infty} \omega \hat{a}_n^{\dagger}(\omega) \hat{a}_n(\omega) d\omega \quad (34)$$

and

$$\hat{H}_{\text{int}} \approx \hbar z_0 \sum_{n,n'} \iint \frac{\sqrt{kk'}}{2\pi} \left( \hat{a}_n(\omega) \hat{a}_{n'}^{\dagger}[\omega'] e^{-i(\omega - \omega')t} \beta_{n,n'} + \text{h.c.} \right) d\omega d\omega' \quad (35)$$

where

$$\beta_{nn'} = \iint u_n(x,y) u_{n'}^*(x,y) \phi(x,y) dxdy. \quad (36)$$

To simplify Eq. 35, we assume the laser has center frequency  $\omega_0 = k_0 c$  and that interacting mode frequencies  $\omega$  are confined to a narrow bandwidth  $B \ll \omega_0$  such that  $\sqrt{k\omega_0} \approx k_0$  and  $\int_0^\infty d\omega \approx \int_{-\infty}^\infty d\omega$ . Defining the spatial mode operator [43]

$$\hat{a}_n(t) = \frac{1}{\sqrt{2\pi}} \int_{-\infty}^\infty \hat{a}_n(\omega) e^{-i\omega t} d\omega \quad (37)$$

with commutation relation  $[\hat{a}_n(t), \hat{a}_{n'}(t')] = \delta(t-t')$ , we then find (for notational simplicity, we hereafter use  $a \equiv a(t)$ )

$$H_{\text{int}} \approx \hbar k_0 z_0 \sum_{n,n'} \left( \beta_{n,n'} \hat{a}_n \hat{a}_{n'}^\dagger + \text{h.c.} \right). \quad (38)$$

Equation 38 can be simplified further by choosing a spatial mode basis  $\{u_n\}$  such that the laser mode is  $u_{\text{in}} = u_0$ . Expanding about this mode and keeping only cross terms  $\beta_{n,n'}$  for which  $n \vee n' = 0$  yields a principal mode expansion [32]

$$H_{\text{int}} \approx 2\hbar k_0 z_0 (\beta_{0,0} \hat{a}_0^\dagger \hat{a}_0 + \beta_\perp (\hat{a}_0^\dagger \hat{a}_\perp + \text{h.c.})) \quad (39)$$

where

$$\hat{a}_\perp^\dagger = \beta_\perp^{-1} \sum_{n>0} \beta_{n,0}^* \hat{a}_n^\dagger \quad (40)$$

is an operator describing photon creation in the orthogonal spatial mode  $u_\perp = \sum_{n>0} \beta_{n,0} u_n$  and  $\beta_\perp^2 = \sum |\beta_{n,0}|^2$ .

Going one step further, for each spatial mode operator  $\hat{a}_n$  we can define temporally orthogonal components  $\hat{a}_{n,c}(t)$  and  $\hat{a}_{n,m}(t)$  whose frequency content is centered around the laser frequency  $\omega_0$  and motional sideband frequencies  $\omega_0 \pm \omega_m$ , respectively, with a bandwidth  $B_m$  much smaller than the mechanical frequency  $\omega_m$  and larger than the mechanical linewidth  $\gamma_m$ . Inspecting Eq. 35 with  $z_0(t) \approx z_0 \cos(\omega_m t)$ , it is evident the optomechanical interaction occurs between two spatio-temporally orthogonal (non-commuting) modes

$$\hat{a}_{\text{in}}(t) = \hat{a}_{0,c}(t) \quad (41a)$$

$$\hat{a}_{\text{sc}}(t) = \beta^{-1} \sum \beta_{0,n} \hat{a}_{0,m}(t) \quad (41b)$$

$$\approx \beta^{-1} (\beta_{0,0} \hat{a}_{0,m}(t) + \beta_\perp a_\perp(t)) \quad (41c)$$

$$\equiv \beta^{-1} (\beta_\parallel \hat{a}_\parallel(t) + \beta_\perp \hat{a}_\perp(t)) \quad (41d)$$

with normalization  $\beta^2 = \beta_\parallel^2 + \beta_\perp^2 = \sum_n |\beta_{0,n}|^2$ .

Physically,  $\hat{a}_{\text{sc}}^\dagger$  describes creation of (temporally orthogonal) photons in spatial mode  $u_{\text{sc}}$ , and  $\hat{a}_\parallel^\dagger$  and  $\hat{a}_\perp^\dagger$  describe the fraction created in the incident spatial mode  $u_{\text{in}} = u_0$  and its orthogonal complement  $u_\perp$ , respectively, defined by

$$\begin{aligned} u_{\text{sc}}(x,y) &= \frac{\beta^{-1}}{\sqrt{\langle u_{\text{in}} \phi, u_{\text{in}} \phi \rangle^{-1}}} \underbrace{\sum_n \beta_{n,0} u_n(x,y)}_{\phi u_{\text{in}}} \\ &= \beta^{-1} \left( \underbrace{\beta_{0,0} u_0(x,y)}_{\beta_\parallel u_\parallel} + \underbrace{\sum_{n>0} \beta_{n,0} u_n(x,y)}_{\beta_\perp u_\perp} \right) \end{aligned} \quad (42)$$

Rewriting Eq. 39 in terms of interacting modes with  $z_0$  promoted to an operator  $z_0 \rightarrow \hat{z}$  yields Eq. 5 of the main text:

$$\hat{H}_{\text{int}} = 2\hbar k \beta \hat{z} \left( \hat{a}_{\text{sc}} \hat{a}_{\text{in}}^\dagger + \hat{a}_{\text{sc}}^\dagger \hat{a}_{\text{in}} \right) \quad (43)$$

As a final simplification, we move to a frame rotating at the laser carrier frequency  $\omega_0$  (by replacing  $a \rightarrow a e^{i\omega_0 t}$ ) and assume that the input field is in a strong coherent state,

$$\hat{a}_{\text{in}} \rightarrow \sqrt{N} + \hat{a}_{\text{in}} \quad (44)$$

where here  $N \gg 1$  is the incident photon flux and  $\hat{a}_{\text{in}}$  has been redefined to represent vacuum fluctuations. Substituting Eq. 44 into Eq. 43 and keeping only terms to first order in  $\hat{a}_{\text{in}}$  yields the linearized interaction Hamiltonian used in Eq. 6

$$\hat{H}_{\text{int}} = 2\hbar k \sqrt{N} \beta \hat{X}_{\text{sc}} \hat{z} = 2\hbar k \sqrt{N} (\beta_\parallel \hat{X}_\parallel + \beta_\perp \hat{X}_\perp) \hat{z} \quad (45)$$

where  $\hat{X} = \hat{a}^\dagger + \hat{a}$  is the amplitude operator.

### III. OPTOMECHANICAL EQUATION OF MOTION, INPUT-OUTPUT RELATIONS, AND QUANTUM NOISE

In this section we derive the optomechanical equations of motion and quantum noise spectra discussed in the main text (Eqs. 7-11). Our analysis proceeds from the linearized optomechanical (OM) Hamiltonian in the frame rotating at  $\omega_0$  (Eqs. 44-45), which, ignoring constants and bath terms, and operating in the Heisenberg picture (replacing  $a_n(\omega) e^{-i\omega t} \rightarrow a_n(\omega, t) \equiv a_n(\omega)$  in Eq. 37), can be expressed as

$$\hat{H} = \hat{H}_{\text{EM}}^{\text{free}} + \hat{H}_m + \hat{H}_{\text{int}} \quad (46)$$

$$\approx \int \hbar \omega \left( a_{\text{in}}^\dagger(\omega) a_{\text{in}}(\omega) + a_{\text{sc}}^\dagger(\omega) a_{\text{sc}}(\omega) \right) d\omega$$

$$+ \hbar \omega_m \hat{b}^\dagger \hat{b} + 2\hbar k \sqrt{N} \beta \hat{z} \frac{1}{\sqrt{2\pi}} \int \left( a_{\text{sc}}^\dagger(\omega) + a_{\text{sc}}(\omega) \right) d\omega$$

where  $\hat{b}$  is a bosonic operator for the mechanical oscillator satisfying  $[\hat{b}, \hat{b}^\dagger] = 1$ ,  $\hat{z} = z_{\text{ZP}}(\hat{b}^\dagger + \hat{b})$  is the mechanical displacement operator,  $z_{\text{ZP}} = \sqrt{\hbar/(2m_{\text{eff}}\omega_m)}$  the oscillator's zero-point motion, and  $m_{\text{eff}}$  is its effective mass.

Equations of motion for  $\hat{a}_{\text{sc}}(\omega)$  and  $\hat{b}$  are obtained from the Heisenberg equation of motion  $\hat{O}(t) = (i/\hbar)[\hat{H}, \hat{O}(t)]$ :

$$\dot{\hat{a}}_{\text{sc}}(\omega, t) = -i\omega \hat{a}_{\text{sc}}(\omega, t) - 2ik\sqrt{N}/(2\pi)\beta \hat{z}(t) \quad (47a)$$

$$\dot{\hat{b}}(t) = -i\omega_m \hat{b}(t) - 2ik\sqrt{N}\beta z_{\text{ZP}} \hat{X}_{\text{sc}}(t). \quad (47b)$$

For the field operator, a standard procedure [35, 36, 44] yields the input-output relation (Eq. 7)

$$\hat{a}_{\text{sc}}^{\text{out}}(t) = \hat{a}_{\text{sc}}^{\text{in}}(t) + 2ik\beta\sqrt{N}\hat{z}(t) \quad (48)$$

where  $\hat{a}_{\text{sc}}$  (the output field operator) and  $\hat{a}_{\text{sc},0}$  (the input field operator) represent the scattered field before and after interacting with the membrane at time  $t$ , respectively. Introducing the phase quadrature  $\hat{Y}_{\text{sc}} = i(\hat{a}_{\text{sc}} - \hat{a}_{\text{sc}})$  and rotated quadrature  $\hat{X}_{\text{sc}}^\theta = \hat{X}_{\text{sc}} \cos \theta + \hat{Y}_{\text{sc}} \sin \theta$  likewise yields

$$\hat{X}_{\text{sc}}^{\theta, \text{out}}(t) = \hat{X}_{\text{sc}}^{\theta, \text{in}}(t) - 4k\beta\sqrt{N}z(t) \sin \theta. \quad (49)$$

In the main text, we take  $\hat{X}_{\text{sc}}^{\theta, \text{in}}$  to be vacuum noise.

Equation 49 shows that displacement is encoded into the phase ( $\theta = \pi/2$ ) of the scattered field, while Eq. 47b suggests that backaction arises due to scattered mode amplitude

quantum noise. Substituting  $z_{\text{ZP}}(\hat{b} + \hat{b}^\dagger) = \hat{z}$  yields the equation of motion for mechanical displacement,

$$m\ddot{\hat{z}}(t) + m\dot{\hat{z}}(t)\Gamma_m + m\omega_m^2\hat{z}(t) = \hat{F}_{\text{BA}}(t) + F_{\text{th}}(t) \quad (50)$$

in which backaction manifests as a stochastic force

$$\hat{F}_{\text{BA}} = 2\hbar k\sqrt{N}\beta\hat{X}_{\text{sc}}^{\text{in}} \quad (51)$$

In Eq. 50 we have also introduced thermal noise via an ad-hoc dissipative force (characterized by mechanical damping rate  $\Gamma_m$ ) and the associated thermal force  $F_{\text{th}}$  due to the Fluctuation-Dissipation theorem [45].

In the frequency domain, Eqs. 49 and 50 constitute the optomechanical equations of motion in the main text (Eq. 8)

$$\hat{X}_{\text{sc}}^{\theta,\text{out}}(\omega) = \hat{X}_{\text{sc}}^{\theta,\text{in}}(\omega) - 4k\beta\sqrt{N}z(\omega)\sin\theta \quad (52a)$$

$$m((\omega_m^2 - \omega^2) + i\omega\Gamma_m)\hat{z}(\omega) = \hat{F}_{\text{BA}}(\omega) + F_{\text{th}}(\omega) \quad (52b)$$

$$\equiv \chi(\omega)^{-1}\hat{z}(\omega) \quad (52c)$$

where  $\chi(\omega) = F(\omega)/z(\omega)$  is the mechanical susceptibility.

We now compute the spectra of the optical quadratures and mechanical displacement in units of single-sided PSD  $S_X$  and cross spectral density (CSD)  $S_{XY}$ :

$$S_X(\omega) = 2 \int_{-\infty}^{\infty} \langle \hat{X}^\dagger(t)\hat{X}(0) \rangle e^{-i\omega t} dt \quad (53a)$$

$$S_{XY}(\omega) = 2 \int_{-\infty}^{\infty} \langle \hat{X}^\dagger(t)\hat{Y}(0) \rangle e^{-i\omega t} dt \quad (53b)$$

where  $\langle \hat{X}^*(t)\hat{Y}(0) \rangle$  denotes the cross-correlation of  $X$  and  $Y$ , with the aim of deriving the SQL for active imaging (Eq. 3).

We are specifically interested in the apparent displacement PSD of an ideal homodyne measurement, defined as the displacement-equivalent PSD of the rotated field quadrature

$$S_z^\theta \equiv (16k^2\beta^2N\sin^2\theta)^{-1} S_{X_{\text{sc}}^{\theta}}^{\text{out}}. \quad (54)$$

Using

$$S_{X_{\text{sc}}^{\theta}} = \cos^2\theta S_{X_{\text{sc}}} + \sin^2\theta S_{Y_{\text{sc}}} + 2\sin(2\theta)\text{Re}[S_{X_{\text{sc}}Y_{\text{sc}}}] \quad (55)$$

and expanding the right-hand side of Eq. 54 yields

$$S_z^\theta = \frac{S_{X_{\text{sc}}^{\theta}}^{\text{in}}}{16k^2\beta^2N\sin^2\theta} + S_z + \frac{\sin(2\theta)\text{Re}[S_{X_{\text{sc}}^{\text{out}}Y_{\text{sc}}^{\text{out}}}]}{8k^2\beta^2N\sin^2\theta} \quad (56a)$$

$$= \underbrace{\frac{S_{X_{\text{sc}}^{\theta}}^{\text{in}}}{16k^2\beta^2N\sin^2\theta}}_{S_z^{\text{imp}}} + \underbrace{|\chi|^2 S_F^{\text{BA}}}_{S_z^{\text{BA}}} + \underbrace{|\chi|^2 S_F^{\text{th}}}_{S_z^{\text{th}}} + \underbrace{\frac{\text{Re}[S_{X_{\text{sc}}^{\text{out}}Y_{\text{sc}}^{\text{out}}}]}{4k^2\beta^2N\sin^2\theta}}_{S_z^{\text{imp,BA}}} \quad (56b)$$

where  $S_z^{\text{imp}}$ ,  $S_z^{\text{BA}}$ ,  $S_z^{\text{th}}$ , and  $S_z^{\text{imp,BA}}$  are the PSD of the apparent displacement (imprecision) due to shot noise, physical displacement due to backaction and thermal noise, and the correlation between imprecision and backaction noise, respectively.

Using Eq. 52a and the correlators  $\langle \hat{a}_n(t)\hat{a}_m^\dagger(t') \rangle = \delta_{nm}\delta(t-t')$  and  $\langle \hat{a}_n^\dagger(t)\hat{a}_m(t') \rangle = 0$  yields

$$S_{X_{\text{sc}}^{\theta}}^{\text{in}}(\omega) = 2 \quad (57a)$$

$$S_{X_{\text{sc}}^{\theta}}^{\text{out}}(\omega) = -16\hbar k^2\beta^2N\chi(\omega) \quad (57b)$$

The non-zero CSD is due to the mechanical response to backaction, which couples amplitude and phase fluctuations.

Collecting terms yields

$$S_z^{\text{imp}} = (8k^2\beta^2N\sin^2\theta)^{-1} \quad (58a)$$

$$S_z^{\text{BA}} = 8\hbar^2k^2\beta^2N|\chi|^2 = |\chi|^2 S_F^{\text{BA}} \quad (58b)$$

$$S_z^{\text{imp,BA}} = -4\hbar\cot\theta\text{Re}[\chi] \quad (58c)$$

recovering expressions in the main text. Finally, combining Eqs. 58a and 58b yields Eq. 3 of the main text:  $S_z^{\text{imp}}S_F^{\text{BA}} = \hbar^2$ .

We conclude by deriving Eq. 11 in the main text, describing quantum correlations between the two orthogonal spatial modes comprising the scattered field. To this end, we substitute  $a_{\text{sc}} = \beta^{-1}(\beta_{\parallel}a_{\parallel} + \beta_{\perp}a_{\perp})$  into Eq. 46 and apply an analogous procedure to obtain input-output relations

$$\hat{X}_{\perp}^{\theta,\text{out}}(t) = \hat{X}_{\perp}^{\theta,\text{in}}(t) - 4k_0\beta_{\perp}\sqrt{N}z(t)\sin\theta \quad (59a)$$

$$\hat{X}_{\parallel}^{\theta,\text{out}}(t) = \hat{X}_{\parallel}^{\theta,\text{in}}(t) - 4k_0\beta_{\parallel}\sqrt{N}z(t)\sin\theta \quad (59b)$$

and noise spectra

$$S_{X_{\perp}^{\theta}}^{\text{in}}(\omega) = 2 \quad (60a)$$

$$S_{X_{\perp}^{\theta}Y_{\perp}^{\theta}}^{\text{out}}(\omega) = -16\hbar k^2\beta_{\perp}^2N\chi(\omega) \quad (60b)$$

$$S_{X_{\parallel}^{\theta}Y_{\perp}^{\theta}}^{\text{out}}(\omega) = -16\hbar k^2\beta_{\perp}\beta_{\parallel}N\chi(\omega). \quad (60c)$$

The correlations given by Eq. 60c are a signature of ‘‘ponderomotive entanglement’’ [31]—i.e., correlations between two otherwise independent (in this case spatially orthogonal) optical modes due to their mutual coupling to a mechanical oscillator. To verify entanglement, one can construct EPR-like quadratures of the joint system  $\hat{X}_+ = \hat{X}_{\parallel}^{\theta} + \hat{X}_{\perp}^{\theta}$  and  $\hat{Y}_- = \hat{Y}_{\parallel}^{\theta} - \hat{Y}_{\perp}^{\theta}$ , where  $\hat{Y}^{\theta} = \sin(\theta)\hat{X} + \cos(\theta)\hat{Y}$ . Since the linearized interaction preserves the Gaussianity of its input states, a necessary and sufficient condition for entanglement is the Duan–Giedke–Cirac–Zoller (DGCZ) criterion [30–32],

$$I(\omega) \equiv \frac{S_{X_+}^{\text{out}}(\omega) + S_{Y_-}^{\text{out}}(\omega)}{8} < 1, \quad (61)$$

which here we have normalized to the vacuum state single-sided PSD of 2. Considering the simplified scenario  $\bar{\beta} = \beta_{\parallel} = \beta_{\perp} \neq 0$  and dual homodyne measurements performed on both modes at equal quadrature measurement angles  $\theta$ , we find

$$I(\omega) = 1 + 16k^2\bar{\beta}^2N|\chi|^2(S_F^{\text{BA},\parallel} + S_F^{\text{BA},\perp} + S_F^{\text{th}})\sin^2(\theta) - 16\hbar k^2\bar{\beta}^2N\text{Re}[\chi]\sin(2\theta) \quad (62a)$$

$$= 1 + 16k^2\bar{\beta}^2N\sin^2\theta \left( S_z^{\text{BA}} + S_z^{\text{th}} + S_z^{\text{imp,BA}}/2 \right) \quad (62b)$$

Where  $S_F^{\text{BA},\parallel(\perp)} = (\beta_{\parallel(\perp)}/\beta)^2 S_F^{\text{BA}}$  is the fraction of the backaction force due to temporal (spatial) photon shot noise. For small quadrature angles  $\theta$  in the backaction-dominated regime ( $S_z^{\text{BA}} > S_z^{\text{th}}$ ), the correlation term  $S_z^{\text{imp,BA}}$  produces  $I(\omega) < 1$  near the mechanical resonance. Representative plots of the DGCZ criterion for different  $\theta$  are shown in Fig. 5.

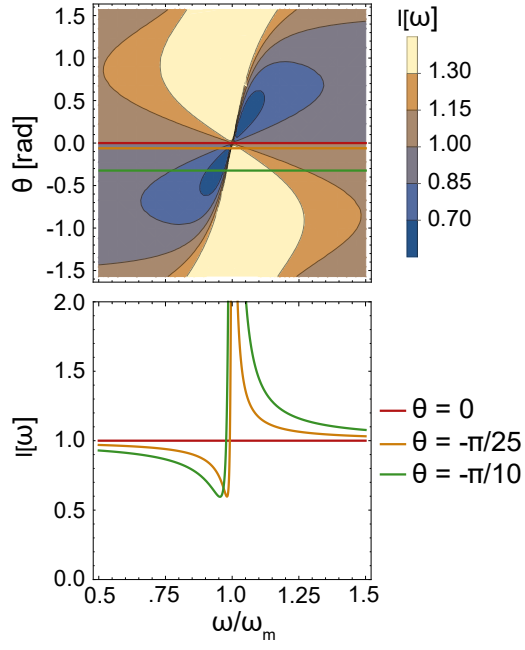


FIG. 5. (a) DGCZ criterion  $I$  (Eq. 62a) versus Fourier frequency  $\omega$  and homodyne phase angle  $\phi$ , with  $\omega_m = 2\pi \times 40$  kHz,  $m = 10^{-12}$  kg,  $\omega_m/\Gamma_m = 4 \times 10^7$ ,  $k^2\beta^2N = 2\pi^2 \times 10^{24} \text{ m}^{-2} \text{ s}^{-1}$ , and zero bath temperature ( $S_z^{\text{th}} = 2\hbar\omega_m\Gamma_m m|\chi|^2$ ). (b) Cuts of the along three phase angles, corresponding to horizontal lines in (b).